Efficient method for grand-canonical twist averaging in quantum Monte Carlo calculations

Sam Azadi [1,2,*] and W. M. C. Foulkes [2]

[1]*Department of Physics, King's College London, Strand, London WC2R 2LS, United Kingdom*
[2]*Department of Physics, Imperial College London, South Kensington Campus, London SW7 2AZ, United Kingdom*

We introduce a simple but efficient method for grand-canonical twist averaging in quantum Monte Carlo calculations. By evaluating the thermodynamic grand potential instead of the ground-state total energy, we greatly reduce the sampling errors caused by twist-dependent fluctuations in the particle number. We apply this method to the electron gas and to metallic lithium, aluminum, and solid atomic hydrogen. We show that, even when using a small number of twists, grand-canonical twist averaging of the grand potential produces better estimates of ground-state energies than the widely used canonical twist-averaging approach.

I. INTRODUCTION

Many-body wave-function-based quantum Monte Carlo (QMC) techniques such as variational Monte Carlo, diffusion Monte Carlo (DMC), and auxiliary field Monte Carlo are widely used to calculate ground- and excited-state properties of real materials [1–11]. Many materials and properties that cannot be described accurately using single-particle-based approaches have been studied successfully using QMC methods. For example, QMC techniques have been used to elucidate the nature of noncovalent and weak van der Waals interactions, which are crucial in chemistry, biology, and biochemistry [3]. The most important contribution of QMC to materials science and electronic structure theory has perhaps been to provide input to mean-field-based methods, most notably via the QMC calculations of the homogeneous electron gas [12] that led to the first accurate local density approximation and have directly or indirectly contributed to almost every exchange-correlation functional devised since then.

QMC calculations of the properties of crystals and solids use finite simulation cells subject to periodic boundary conditions. The volume of the simulation cell is strongly restricted for computational reasons, and the finite-size errors caused by the replacement of an infinite solid by a small simulation cell are large. Controlling these errors is one of the main challenges faced in all QMC simulations of extended systems [13–17].

Within the Born-Oppenheimer approximation, the Hamiltonian of an N-electron simulation cell can be expressed as $\hat{H} = \hat{T} + \hat{V}$, where $\hat{T}$ is the electronic kinetic-energy (KE) operator and $\hat{V}$ is the operator for the interaction energy, including electron-electron and electron-nuclear contributions: $\hat{V} = \hat{V}_{\text{e-e}} + \hat{V}_{\text{e-n}}$. The expectation value of $\hat{V}_{\text{e-e}}$ is often written as the sum of two terms: $\langle \hat{V}_{\text{e-e}} \rangle = E_{\text{H}} + E_{xc}$. The Hartree energy E_{H} is the classical Coulomb interaction energy associated with the electronic charge density $\rho_e(\mathbf{r})$. The exchange-correlation energy E_{xc} contains the rest of the electron-

electron interaction energy, including contributions from the correlations between the positions of electrons and the antisymmetry of the fermionic many-electron wave function. The electron-nuclear interaction energy $\langle \hat{V}_{\text{e-n}} \rangle$ and the Hartree energy E_{H} are functionals of the electronic charge density $\rho_e(\mathbf{r})$, which normally converges rapidly as the number of unit cells within the simulation cell increases. Thus, the finite-size errors in these terms are small compared to those in other components of the total energy. By contrast, the finite-size errors in the exchange-correlation energy and the KE can be very substantial. In this work, we introduce an efficient and practical method for correcting the finite-size errors in the dominant one-electron contribution to the KE.

II. SINGLE-PARTICLE FINITE-SIZE PROBLEM

In mean-field-like approaches such as density functional theory (DFT), exact results for infinite periodic crystals can be obtained by solving the Schrödinger equation within a single primitive unit cell subject to Bloch boundary conditions. Expectation values per unit cell of the infinite periodic system are obtained by integrating over the first Brillouin zone, which is equivalent to averaging over all possible Bloch boundary conditions.

This approach does not yield exact results in many-particle methods such as QMC. The problem is that the range of the correlations between electron positions often exceeds the size of the primitive unit cell. Reducing the system to one primitive cell is then no longer acceptable. QMC simulations are instead carried out in simulation cells comprising several primitive cells. Exact results are obtained only in the limit as the size of the simulation cell tends to infinity.

The long-range many-body correlation effects are included in an approximate way in local and semilocal DFT calculations, where they are built into the exchange-correlation functional. This functional, however, was parameterized with the help of QMC simulations of large simulation cells.

Generally, in QMC calculations of periodic systems, the Hamiltonian $\hat{H}$ of the N-electron simulation cell exhibits two

*sam.azadi@kcl.ac.uk

types of periodicity [18]:

$$\hat{H}(\mathbf{r}_1, \ldots, \mathbf{r}_i, \ldots, \mathbf{r}_N) = \hat{H}(\mathbf{r}_1, \ldots, \mathbf{r}_i + \mathbf{R}_s, \ldots, \mathbf{r}_N) \quad (1)$$

for all $1 \leqslant i \leqslant N$ and

$$\hat{H}(\mathbf{r}_1, \mathbf{r}_2, \ldots, \mathbf{r}_N) = \hat{H}(\mathbf{r}_1 + \mathbf{R}_p, \mathbf{r}_2 + \mathbf{R}_p, \ldots, \mathbf{r}_N + \mathbf{R}_p), \quad (2)$$

where $\mathbf{R}_s$ and $\mathbf{R}_p$ are the simulation-cell and primitive-cell lattice vectors, and $(\mathbf{r}_1, \mathbf{r}_2, \ldots, \mathbf{r}_N)$ are the electron coordinates. The simulation-cell periodicity, Eq. (1), arises from the periodic boundary conditions applied across the finite simulation cell and does not hold in a real solid; the primitive-cell periodicity, Eq. (2), also holds in real systems as long as periodic boundary conditions are applied to the solid as a whole.

Because of the two types of periodicity, the N-electron wave function of the simulation cell obeys two types of Bloch's theorem:

$$\Psi_{\mathbf{k}_s} = V_{\mathbf{k}_s}(\mathbf{r}_1, \ldots, \mathbf{r}_N) \exp\left(i\mathbf{k}_s \cdot \sum_{i=1}^{N} \mathbf{r}_i\right), \quad (3)$$

$$\Psi_{\mathbf{k}_p} = U_{\mathbf{k}_p}(\mathbf{r}_i, \ldots, \mathbf{r}_N) \exp\left(i\mathbf{k}_p \cdot \frac{1}{N}\sum_{i=1}^{N} \mathbf{r}_i\right), \quad (4)$$

where $V_{\mathbf{k}_s}$ is invariant under the translation of any one electron by a simulation-cell lattice vector $\mathbf{R}_s$ and $U_{\mathbf{k}_p}$ is invariant under the simultaneous translation of all N electrons by a primitive lattice vector $\mathbf{R}_p$. Without loss of generality, we can assume that the simulation-cell wave vector $\mathbf{k}_s$ lies within the simulation-cell Brillouin zone and that the primitive Bloch wave vector $\mathbf{k}_p$ lies within the primitive Brillouin zone (which is, of course, larger).

A many-body simulation with a nonzero $\mathbf{k}_s$ is normally described as being subject to twisted boundary conditions [19], and averaging the results over different twists is called twist averaging. The technique of twist averaging can be carried out in the canonical ensemble (CE), which fixes the number of electrons in the simulation cell, or in the grand-canonical ensemble (GCE), which allows the number of electrons to vary with the twist $\mathbf{k}_s$. Because of the existence of a sharp Fermi surface and shell-filling effects, the use of twisted boundary conditions is more important in metals than in insulators [19].

To clarify the origin of the shell-filling effects, consider a finite simulation cell of noninteracting electrons subject to twisted boundary conditions. The one-electron potential has the periodicity of the primitive unit cell, so the single-particle orbitals adopt the usual Bloch form, $\psi_{\mathbf{k}} = u_{\mathbf{k}}(\mathbf{r}) \exp(i\mathbf{k} \cdot \mathbf{r})$, where $u_{\mathbf{k}}(\mathbf{r})$ has the periodicity of the primitive cell. The twisted boundary conditions require the Bloch wave vector to lie on a grid of points of the form $\mathbf{k} = \mathbf{k}_s + \mathbf{G}_s$, where $\mathbf{G}_s$ is a reciprocal vector of the simulation-cell lattice. There are exactly N_c such reciprocal vectors within the primitive Brillouin zone, where N_c is the number of primitive unit cells in the simulation cell. To make this more concrete, consider a simulation cell consisting of $N_c = L \times L \times L$ primitive unit cells. The Bloch wave vectors then lie on an $L \times L \times L$ Monkhorst-Pack grid [20] within the primitive Brillouin zone, offset from the origin by the twist $\mathbf{k}_s$, which lies within the simulation-cell Brillouin zone.

To calculate, for example, the total noninteracting KE at twist $\mathbf{k}_s$, a sum over contributions from the occupied orbitals at all N_c distinct $\mathbf{k}$ points of the form $\mathbf{k}_s + \mathbf{G}_s$ is carried out. In an infinite simulation cell, the sum becomes an integral over the Brillouin zone, including contributions from every single-particle orbital below the Fermi energy E_f. The grid of simulation-cell reciprocal lattice vectors $\mathbf{G}_s$ becomes finer as the size of the simulation cell increases, so the integrand is sampled more finely for larger simulation cells. In an insulator, where the integrand is a smooth function of $\mathbf{k}$, a coarse quadrature grid is sufficient to yield accurate results, but in metals, where the bands that cross the Fermi level are occupied in some parts of the Brillouin zone and unoccupied in others, the integrand is discontinuous, and the quadrature errors are large. It is then necessary to increase the size of the simulation cell or average over more twists to obtain accurate results.

In noninteracting systems, these two approaches (increasing the size of the simulation cell or averaging over more twists) are equivalent, and both are capable of giving exact results. In interacting systems, increasing the size of the simulation cell still gives exact results, but averaging over twists applied to a finite simulation cell does not. Because of the long-range electronic correlations, no many-body simulation for a finite simulation cell can be exact. In practice, we make the simulation cell as large as computational limitations allow and twist average to reduce the single-particle contributions to the size error. The residual many-body size errors, which are not removed by twist averaging results for a finite simulation cell, are tackled using other methods [13–16].

In QMC simulations of spin-unpolarized systems, the canonical twist-averaging approach works as follows. For every twist $\mathbf{k}_s$, one constructs the determinantal part of the QMC trial wave function by collecting the one-electron orbitals (usually obtained from a DFT or Hartree-Fock calculation) associated with all N_c points on the quadrature grid of points of the form $\mathbf{k} = \mathbf{k}_s + \mathbf{G}_s$. The $N/2$ orbitals of lowest energy are then doubly occupied. This guarantees that the number of electrons in the simulation cell is independent of twist $\mathbf{k}_s$ and always equal to N. In the grand-canonical twist-averaging approach, only those one-electron orbitals for which the mean-field (DFT or Hartree-Fock) energy eigenvalue lies below the mean-field Fermi energy are doubly occupied. Hence, the number of electrons depends on $\mathbf{k}_s$.

In noninteracting systems, grand-canonical twist averaging is exactly equivalent to conventional Brillouin zone integration, which also considers contributions only from orbitals within the Fermi surface. As the number of twists tends to infinity, exact results are obtained. Canonical twist averaging occasionally occupies orbitals outside the Fermi surface and occasionally leaves orbitals within the Fermi surface unoccupied. Assuming that the curvature of the bands crossing the Fermi energy is positive, this add a small positive bias to the energy estimate, even in a noninteracting system.

III. GRAND-CANONICAL TWIST AVERAGING OF THE GRAND POTENTIAL

The conventional grand-canonical twist-averaging method is not generally viewed as a practical approach because of the

strong sensitivity of the total energy of the simulation cell to the twist. This is primarily due to the $\mathbf{k}_s$ dependence of the number of electrons within the simulation cell. It is difficult to get accurate results without sampling impractically large numbers of twists [15,16].

To reduce the cost of twist averaging in the CE, various techniques based on the selection of optimal twists have been used [18,21,22]. In this section, we introduce a different approach to twist averaging in the GCE, allowing total, kinetic, exchange, and correlation energies to be obtained accurately without using very many twists. The uncertainties in results obtained using this GCE twist-averaging algorithm are comparable to those in CE twist-averaging calculations. Unlike CE twist averaging, however, GCE twist averaging removes independent-particle finite-size errors exactly as the number of twists tends to infinity, even for small simulation cells. GCE twist averaging is thus, in general, to be preferred to CE twist averaging.

Quantum Monte Carlo simulations of lattice models in the grand-canonical and canonical ensembles were compared recently [23,24], and it was shown that results obtained using the grand-canonical ensemble converge more rapidly with system size. Grand-canonical twist averaging was also employed as part of a QMC-based approach for estimating the fundamental gap of insulators [25]. An approach similar to ours was previously used to control the finite-size errors in exact diagonalization studies of the one- and two-dimensional Hubbard model [26–28], and Ref. [21] suggests the use of an analogous technique in QMC. We are not aware of any previous attempts to use this idea to improve the efficiency of grand-canonical twist averaging in continuum QMC simulations.

In the conventional GCE twist-averaging approach, results are obtained by twist averaging the total energy,

$$E = \frac{1}{M} \sum_{\mathbf{k}_s} E(\mathbf{k}_s), \tag{5}$$

where the sum is over the sample of M twist vectors $\mathbf{k}_s$ and $E(\mathbf{k}_s)$ is the total energy for twist $\mathbf{k}_s$. If we consider a Hartree-Fock calculation with only a single band for simplicity, $E(\mathbf{k}_s)$ is the energy of the Slater determinant containing all one-electron orbitals $\psi_{\mathbf{k}_s+\mathbf{G}_s}(\mathbf{r})$, with $\mathbf{k}_s$ fixed and $\mathbf{G}_s$ chosen such that $|\mathbf{k}_s + \mathbf{G}_s|$ lies within the Fermi surface.

Energies obtained using Eq. (5) are inaccurate for small numbers of twists because the number of orbitals in the Slater determinant is surprisingly sensitive to the twist $\mathbf{k}_s$. If, for example, we consider a uniform electron gas with $r_s = 1$, choosing the system size such that the fcc simulation cell contains 118 electrons on average, the actual electron number varies from 102 to 128 (at least) as $\mathbf{k}_s$ varies. These $\pm 10\%$ fluctuations in particle number yield similarly large fluctuations in the values of $E(\mathbf{k}_s)$ and hence slow convergence of the mean E with the number of twists.

The observation that leads to a better algorithm is that the thermodynamic free energy appropriate for use with the grand-canonical ensemble is not the internal energy E but the grand potential,

$$\Omega(T, V, \mu) = E(S, V, N) - TS - \mu N, \tag{6}$$

where the entropy S and particle number N appearing on the right-hand side are to be regarded as functions of the temperature T, the volume V, and the chemical potential μ. Since we are working at zero temperature and fixed volume, we simplify this to

$$\Omega(\mu) = E(N) - \mu N. \tag{7}$$

The clearest way to formulate the Legendre transformation that yields $\Omega(\mu)$ from $E(N)$ is to start with a function of *two* independent variables, μ and N,

$$\Omega(\mu, N) = E(N) - \mu N, \tag{8}$$

and define $\Omega(\mu)$ via a minimization:

$$\Omega(\mu) = \text{Min}_N \Omega(\mu, N) = \text{Min}_N(E(N) - \mu N). \tag{9}$$

This variational definition shows explicitly that the free energy Ω is a function of μ, not N, and yields, if we treat N as continuous, the minimization condition,

$$\frac{dE}{dN} = \mu, \tag{10}$$

from which one obtains the function $N(\mu)$ appearing on the right-hand side of Eq. (7).

As in the standard approach to grand-canonical twist averaging, we start by choosing a simulation cell and setting the chemical potential μ. We then calculate the particle numbers $N(\mathbf{k}_s)$ and internal energies $E(\mathbf{k}_s)$ for M different twists $\mathbf{k}_s$. The only new feature is that we average the function of two independent variables, $\Omega(\mu, N) = E(N) - \mu N$, instead of $E(N)$. Since $\Omega(\mu, N)$ is stationary with respect to variations of N about the true particle number $N(\mu)$ at fixed μ, the function $\Omega(\mu, N)$ is relatively insensitive to small changes in N. The values of $\Omega(\mu, N)$ obtained using different twists are therefore good estimates of $\Omega(\mu)$, and the fluctuations in the twist-averaged estimate of the grand potential,

$$\Omega(\mu) = \frac{1}{M} \sum_{\mathbf{k}_s} [E(\mathbf{k}_s) - \mu N(\mathbf{k}_s)], \tag{11}$$

are small.

Once this estimate of $\Omega(\mu)$ has been obtained, the internal energy is easily found using the inverse Legendre transformation

$$E = \Omega + \mu N, \tag{12}$$

where μ is the chosen chemical potential and N is the expected number of electrons in the simulation cell for that value of μ. When applied to a noninteracting system, this grand-potential twist-averaging approach and the standard GCE twist-averaging approach both yield the exact internal energy as the number of twists tends to infinity, regardless of the size of the simulation cell. However, the free-energy-averaging approach yields more accurate results when the number of twists is small.

The chemical potential μ is known because it was chosen, but one might expect the exact value of N corresponding to a given μ to be unknown in an interacting system. If this were the case, the inverse Legendre transformation required to obtain E from Ω could not be carried out exactly in interacting

systems. The most obvious solution to this problem, which is to estimate N via

$$N = \frac{1}{M} \sum_{\mathbf{k}_s} N(\mathbf{k}_s), \tag{13}$$

is no good because the resulting internal energy estimate,

$$E = \frac{1}{M} \sum_{\mathbf{k}_s} [E(\mathbf{k}_s) - \mu N(\mathbf{k}_s)] + \frac{\mu}{M} \sum_{\mathbf{k}_s} N(\mathbf{k}_s)$$

$$= \frac{1}{M} \sum_{\mathbf{k}_s} E(\mathbf{k}_s), \tag{14}$$

reduces to Eq. (5), reintroducing the sensitivity to twist and concomitant large fluctuations.

Fortunately, in any practical example, even for a correlated calculation, we *do* know the mean value of N corresponding to any given μ. The Slater determinant part of the Slater-Jastrow trial function for a given twist contains exactly the same number of electrons as the corresponding mean-field wave function, and the Jastrow factor does not change this. The mean value of N, as obtained by an infinitely dense twist sampling, is thus exactly the same as in the mean-field case and is easily expressed in terms of the volume of the mean-field Fermi surface:

$$N = \frac{V}{(2\pi)^3} \sum_n \int_{BZ} H[\mu - \epsilon_n(\mathbf{k})] \, d^3k, \tag{15}$$

where V is the volume of the simulation cell, the summation is over the band index n, the integral is over the primitive Brillouin zone (BZ), $H(x)$ is the Heaviside step function [$H(x) = 0, x < 0; H(x) = 1, x > 0$], and $\epsilon_n(\mathbf{k})$ is the mean-field one-electron eigenvalue of band n at Bloch wave vector $\mathbf{k}$.

The chosen value of the chemical potential μ is, in practice, taken from the same DFT or Hartree-Fock calculation used to obtain the one-electron orbitals, so the DFT or Hartree-Fock code ensures that the Brillouin zone integral above yields exactly the right number of electrons per unit cell. This means that we already know the value of N corresponding to the chosen chemical potential μ and do not need to evaluate the Brillouin zone integral again. In the next section, for example, we report results for a simulation cell containing 96 aluminum atoms, each with 3 valence electrons. The value of μ obtained from the DFT code is such that N is exactly $96 \times 3 = 288$.

The mean-field chemical potential μ is not precisely equal to dE/dN when E is the fully correlated energy. Consequently, $\Omega(\mu, N)$ will not be exactly stationary with respect to small variations of N about its mean and the twist sensitivity of $\Omega(\mu, N)$ will be increased. As long as the mean-field estimate of μ is reasonably close to the true interacting chemical potential, however, the fluctuations about the mean should still be much smaller than in the internal-energy-based GCE twist-averaging approach. Furthermore, even when the estimate of μ is inaccurate and the sensitivity of the grand potential to the twist is large, the fully twist averaged energy expectation value remains exact. The free-energy-based GCE twist-averaging algorithm therefore works almost as well in fully correlated QMC simulations as in mean-field calculations.
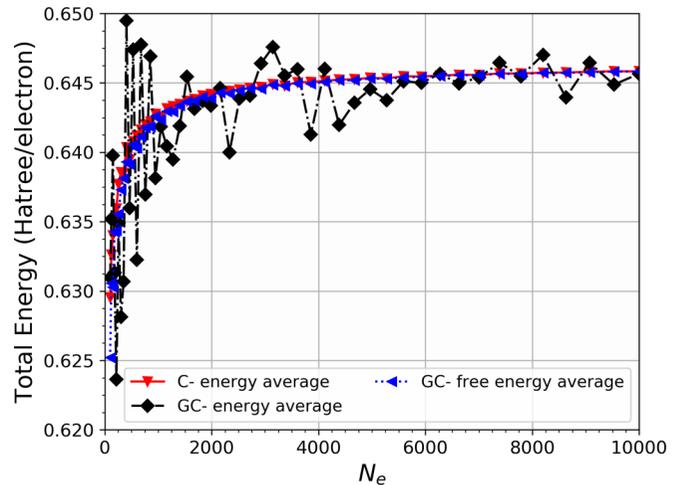

FIG. 1. System-size dependence of the calculated total energy per electron of an $r_s = 1$ uniform electron gas in the Hartree-Fock approximation. Results obtained using canonical twist averaging of the total energy, grand-canonical twist averaging of the total energy, and grand-canonical twist averaging of the grand potential (free energy) are shown. In all cases, a $3 \times 3 \times 3$ grid of twists centered on the Γ point was used.

It is reassuring to note that the free-energy-based GCE twist-averaging method yields exactly the same results as the internal-energy-based GCE sampling method in the limit as the number of twists M tends to infinity, regardless of the accuracy of the estimate of μ employed. Averaging the free energy reduces the fluctuations but does not affect the final estimate of the internal energy when the twist grid is fine enough.

IV. RESULTS

A. Uniform electron gas

This section compares results obtained by applying three different twist-averaging methods to the uniform electron gas with $r_s = 1$. The energies were calculated in the mean-field Hartree-Fock approximation, so twist averaging is here being used as an alternative to conventional Brillouin-zone averaging of mean-field results. All calculations used a Monkhorst-Pack grid of only $3 \times 3 \times 3$ twists (not all inequivalent) centered on the Γ point of the simulation-cell Brillouin zone.

Figure 1 shows that the "random errors" associated with the grand-canonical free-energy averaging algorithm are much smaller than those associated with the grand-canonical internal energy averaging algorithm and no larger than those associated with canonical twist averaging of the internal energy. The systematic error is dominated by the long-range Coulomb contribution to the exchange energy, which cannot be removed by twist averaging [13,15], but the additional small positive bias caused by the approximation of the Fermi surface implicit in the canonical twist-averaging algorithm can, nevertheless, be resolved.

As can be seen in Figs. 2 and 3, the free-energy-based GCE twist-averaging method works just as well for the kinetic energy, the exchange energy, and, presumably, also other
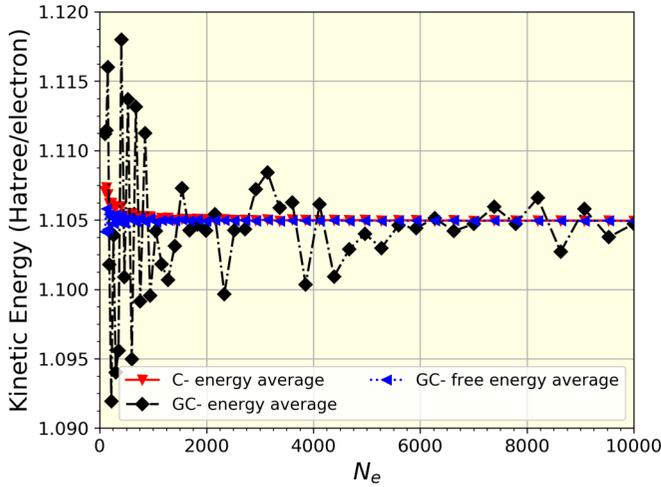
FIG. 2. System-size dependence of the calculated kinetic energy per electron of an $r_s = 1$ uniform electron gas in the Hartree-Fock approximation. Results obtained using canonical twist averaging of the kinetic energy, grand-canonical twist averaging of the kinetic energy, and grand-canonical twist averaging of the kinetic component of the grand potential are shown. In all cases, a $3 \times 3 \times 3$ grid of twists centered on the Γ point was used.

components of the total energy. To obtain the kinetic and exchange energies, one averages the kinetic and exchange components of the grand potential,

$$\Omega_T = \frac{1}{M} \sum_{\mathbf{k}_s} [T(\mathbf{k}_s) - \mu_T N(\mathbf{k}_s)], \tag{16}$$

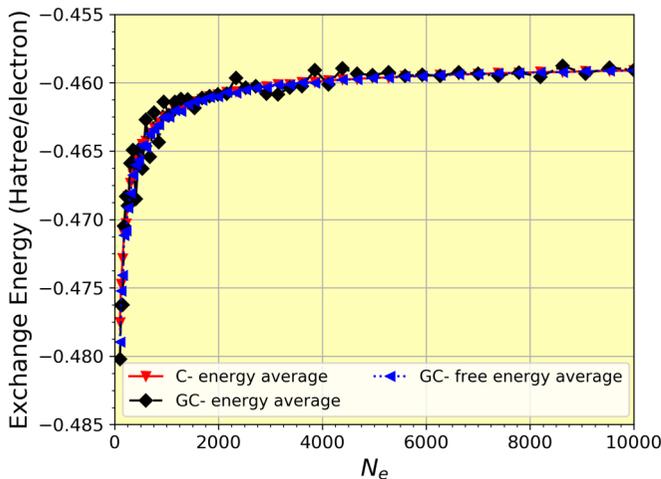$$\Omega_{E_x} = \frac{1}{M} \sum_{\mathbf{k}_s} [E_x(\mathbf{k}_s) - \mu_{E_x} N(\mathbf{k}_s)], \tag{17}$$

FIG. 3. System-size dependence of the calculated exchange energy per electron of an $r_s = 1$ uniform electron gas in the Hartree-Fock approximation. Results obtained using canonical twist averaging of the exchange energy, grand-canonical twist averaging of the exchange energy, and grand-canonical twist averaging of the exchange component of the grand potential are shown. In all cases, a $3 \times 3 \times 3$ grid of twists centered on the Γ point was used.

where $T(\mathbf{k}_s)$ is the kinetic energy of the simulation cell with twist $\mathbf{k}_s$, μ_T is the kinetic contribution to the chemical potential, $E_x(\mathbf{k}_s)$ is the exchange energy of the simulation cell with twist $\mathbf{k}_s$, and μ_{E_x} is the exchange contribution to the chemical potential. For the Hartree-Fock free-electron gas calculations carried out here, μ_T and μ_{E_x} are given (in Hartree atomic units) by $\mu_T = \frac{1}{2}k_f^2$ and $\mu_{E_x} = -\frac{1}{\pi}k_f$, where k_f is the Fermi wave vector.

B. Real metallic systems

This section investigates the value of grand-canonical grand-potential twist averaging in DMC simulations of real metals.

The DMC calculations were carried out using the CASINO QMC package [29] with Slater-Jastrow trial wave functions and the Ewald method for treating the long-range Coulomb interactions. The one-electron orbitals appearing in the Slater determinants were generated within DFT using the QUANTUM ESPRESSO plane-wave code [30] with Trail-Needs Dirac-Fock pseudopotentials [31,32]. The Perdew-Burke-Ernzerhof generalized gradient approximation exchange-correlation functional [33] was used, and the plane-wave cutoff energy was set to 400 Ry to obtain results close to the complete basis-set limit [34]. For Brillouin-zone integrations in metallic systems, we used the Gaussian smearing scheme with the spreading parameter set to 25 meV. The plane-wave representations of the one-electron orbitals were transformed into a blip polynomial basis [35], which is faster to evaluate in QMC simulations. The Jastrow function consisted of polynomial one-body electron-nucleus and two-body electron-electron terms, the parameters of which were optimized by variance minimization at the variational Monte Carlo level [36,37]. We found the effect of reoptimizing the Jastrow correlation function for every different twist to be negligible, so the same optimized Jastrow function was used for all twists. In all DMC calculations a time step of $\tau = 0.005$ hartree atomic units of time was used.

Unlike the twists $\mathbf{k}_s$ used to obtain the electron gas results described in Sec. IV A, which were on a uniform Monkhorst-Pack [20] grid within the simulation-cell Brillouin zone, the twists used for the QMC simulations of real materials reported here were chosen randomly. Since the twists are chosen randomly, the twist-dependent changes in the total energy may be treated as random variables. The chemical potential μ was estimated from DFT calculations. To ensure that the estimate of the DFT Fermi energy was accurate, a dense $24 \times 24 \times 24$ $\mathbf{k}$-point mesh was used.

When applying grand-canonical twist averaging to real metallic systems at zero temperature, we set the chemical potential μ to the single-particle Fermi energy of the infinite system. As explained above, errors in the value of μ increase the twist-dependent fluctuations in the grand potential but do not affect the twist-averaged energy, so the small difference between our choice of μ and the true interacting chemical potential is unimportant. We applied the grand-potential twist-averaging method to three metallic solids: high-pressure atomic hydrogen in the tetragonal crystal structure with $I4_1/amd$ symmetry [38], lithium in the fcc structure [39], and fcc aluminum. The numbers of atoms in the simulation cells
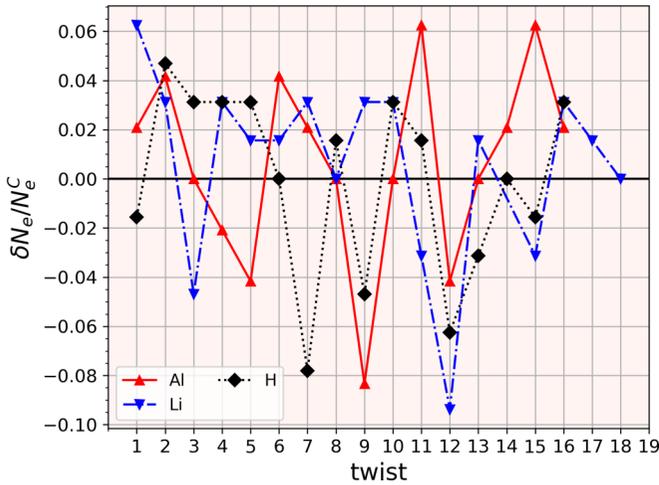
FIG. 4. Relative fluctuations in the number of electrons in the grand-canonical simulation cell: $\delta N_e = N_e^C - N_e^{GC}$, where N_e^C is the number of electrons occupying the simulation cell in the canonical ensemble and N_e^{GC} is the number in the grand-canonical ensemble.

employed for the H, Li, and Al simulations were 128, 128, and 96, respectively. We used 16 random twists for H and Al and 18 random twists for Li.

Various exotic predictions have been made for atomic metallic hydrogen, such as stability in a superfluid state or as a room-temperature superconductor [40,41]. Calculation of the phase diagram of hydrogen and its electronic structure under extreme conditions is a challenging subject for first-principles methods, not least because the results obtained using DFT are severely affected by the choice of exchange-correlation functional [42–44]. The limitations of DFT make DMC simulations of solid hydrogen particularly valuable, but the accuracy required is very high, and controlling the DMC finite-size corrections is an important issue. This is particularly the case when DMC is used to investigate the phase diagram.

Figure 4 shows the relative fluctuations in the number of electrons in the grand-canonical simulation cell as a function of twist vector. The numbers of electrons per atom averaged over the 16 random twists for H and Al and 18 random twists for Li may be evaluated as in Eq. (13). The results are 2.98(2), 0.99(2), and 1.00(1), for Al, Li, and H, respectively. As the number of twists increases, the average number of electrons per atom converges to the number of valence electrons per atom as specified by the pseudopotential. Figure 5 shows our DMC results for metallic H, Li, and Al. The horizontal axis indexes the twists used, and the vertical axis shows the total internal energy per atom for that twist. The red triangles [$E_c(\mathbf{k}_s)$] are energies calculated in the canonical ensemble, with the number of electrons in the simulation cell fixed. The black diamonds [$E_{gc}^{EM}(\mathbf{k}_s)$] are energies calculated in the grand-canonical ensemble, with the number of electrons in the simulation cell dependent on the twist vector. The superscript EM stands for "energy method," indicating that these results were not obtained using the grand potential. As expected, the grand-canonical energy per atom is considerably more sensitive to the twist than the canonical energy per atom.
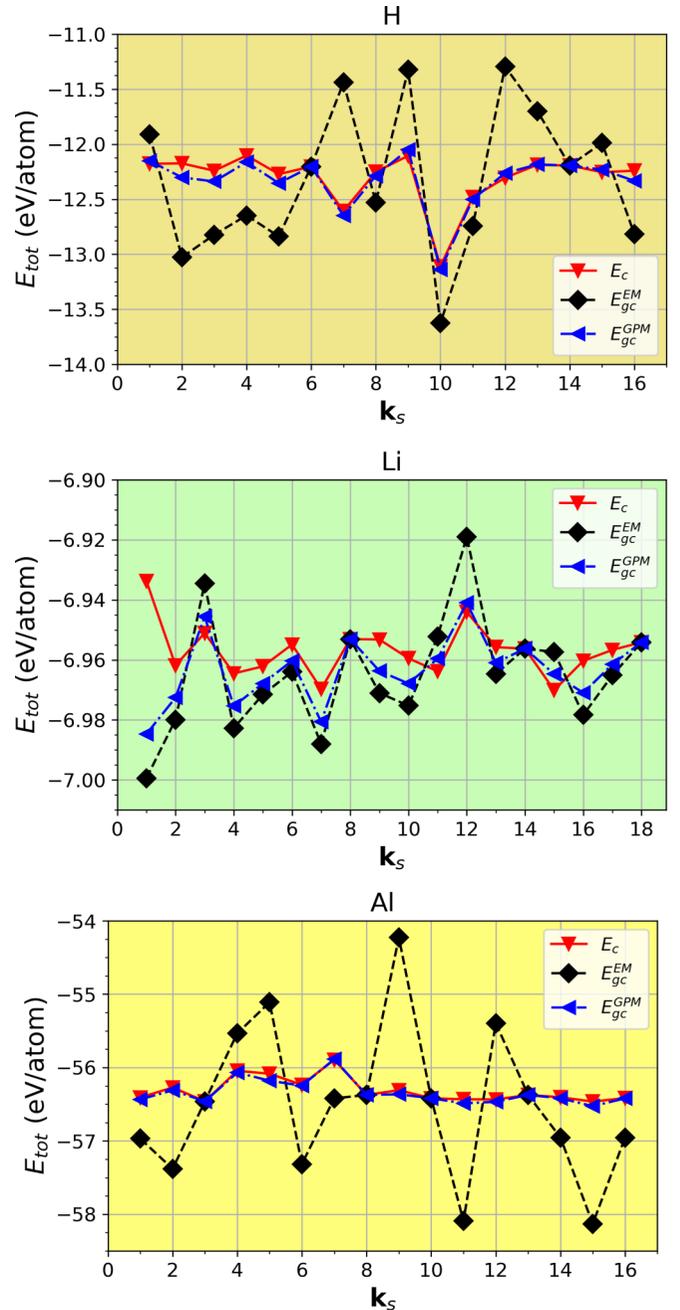

FIG. 5. Twist dependence of the total DMC energy per atom for metallic H in the $I4_1/amd$ structure, fcc Li, and fcc Al. The red triangles are internal energies E_c calculated using canonical simulations in which the number of electrons in the simulation cell is fixed. The black diamonds are internal energies E_{gc}^{EM} calculated using grand-canonical simulations in which the number N_e of electrons in the simulation cell depends on the twist $\mathbf{k}_s$. The blue triangles are energies which are calculated by $E_{gc}^{GPM} = \Omega(\mathbf{k}_s, N_s) + \mu\langle N_e \rangle$ where $\Omega(\mathbf{k}_s, N_s)$ is the grand-canonical potential defined as $E_{gc}^{EM} - \mu N_e(\mathbf{k}_s)$ and $\langle N_e \rangle$ is the average number of electrons. The statistical errors in all data points are smaller than the symbols.

The blue triangles in Fig. 5 are energies calculated using the grand-potential method (GPM):

$$E_{gc}^{GPM}(\mathbf{k}_s) = \Omega(\mathbf{k}_s, N(\mathbf{k}_s)) + \mu\langle N \rangle, \qquad (18)$$

TABLE I. The lattice parameters used (in Å) and total energies (in eV/atom of metallic H, Li, and Al) obtained using canonical twist averaging (E_c), grand-canonical twist averaging of the internal energy (E_{gc}^{EM}), and grand-canonical twist averaging of the grand potential (E_{gc}^{GPM}). When working in the grand-canonical ensemble, twist averaging the grand potential is much more efficient than twist averaging the internal energy.

System	a	c/a	E_c	E_{gc}^{EM}	E_{gc}^{GPM}
H	1.21	2.55	$-12.31(6)$	$-12.3(2)$	$-12.33(6)$
Li	3.21	1.0	$-6.957(2)$	$-6.965(5)$	$-6.964(3)$
Al	4.01	1.0	$-56.31(4)$	$-56.5(3)$	$-56.51(4)$

where

$$\Omega(\mathbf{k}_s, N(\mathbf{k}_s)) = E_{gc}^{EM}(\mathbf{k}_s) - \mu N(\mathbf{k}_s) \tag{19}$$

is the estimate of the grand potential per atom at twist $\mathbf{k}_s$ and $\langle N \rangle$ is the average number of electrons per atom as defined by the pseudopotential. The standard deviation of E_{gc}^{GPM} is much smaller than that of E_{gc}^{EM} for all of the cases studied, but especially for Al, which has a larger number of electrons in the simulation cell.

The twist-averaged DMC energies for each system are reported in Table I. In all three metals the grand-canonical twist-averaged energy lies below the canonical twist-averaged energy. Because all three twist-averaging methods made use of the same random set of twists, the statistical errors in energy differences are likely to be considerably smaller than those in total energies.

V. CONCLUSION

This paper presented a simple but efficient approach to twist averaging in the grand-canonical ensemble. We explained that it is better to average the grand potential $\Omega(\mu)$ than the internal energy. Once the average of the grand potential has been found, the internal energy can be obtained via a Legendre transformation, $E(N) = \Omega(\mu) + \mu N$, where μ is the chosen chemical potential and N is the exact number of electrons per simulation cell. Unlike conventional grand-canonical twist averaging of the internal energy, the grand-potential approach does not require very large numbers of twists to provide accurate total energies, and unlike conventional canonical twist averaging, the results are not biased when the simulation cell is small. This makes grand-potential twist averaging in the grand-canonical ensemble suitable for use in simulations of real metallic systems, where the computational cost is a crucial factor.

[1] W. M. C. Foulkes, L. Mitas, R. J. Needs, and G. Rajagopal, Rev. Mod. Phys. **73**, 33 (2001).

[2] J. Kolorenč and L. Mitas, Rep. Prog. Phys. **74**, 026502 (2011).

[3] M. Dubecký, L. Mitas, and P. Jurečka, Chem. Rev. **116**, 5188 (2015).

[4] M. A. Morales, R. Clay, C. Pierleoni, and D. M. Ceperley, Entropy **16**, 287 (2014).

[5] L. K. Wagner and D. Ceperley, Rep. Prog. Phys. **79**, 094501 (2016).

[6] F. Becca and S. Sorella, *Quantum Monte Carlo Approaches for Correlated Systems* (Cambridge University Press, Cambridge, 2017).

[7] G. H. Booth, A. Grüneis, G. Kresse, and A. Alavi, Nature (London) **493**, 365 (2013).

[8] A. Zen, J. G. Brandenburg, J. Klimeš, A. Tkatchenko, D. Alfè, and A. Michaelides, Proc. Natl. Acad. Sci. USA **115**, 1724 (2018).

[9] S. Sorella, Phys. Rev. B **84**, 241110(R) (2011).

[10] K. Seki and S. Sorella, Phys. Rev. B **99**, 144407 (2019).

[11] M. Motta, S. Zhang, and G. K.-L. Chan, Phys. Rev. B **100**, 045127 (2019).

[12] D. M. Ceperley and B. J. Alder, Phys. Rev. Lett. **45**, 566 (1980).

[13] L. M. Fraser, W. M. C. Foulkes, G. Rajagopal, R. J. Needs, S. D. Kenny, and A. J. Williamson, Phys. Rev. B **53**, 1814 (1996).

[14] S. Chiesa, D. M. Ceperley, R. M. Martin, and M. Holzmann, Phys. Rev. Lett. **97**, 076404 (2006).

[15] N. D. Drummond, R. J. Needs, A. Sorouri, and W. M. C. Foulkes, Phys. Rev. B **78**, 125106 (2008).

[16] M. Holzmann, R. C. Clay, III, M. A. Morales, N. M. Tubman, D. M. Ceperley, and C. Pierleoni, Phys. Rev. B **94**, 035126 (2016).

[17] S. Azadi and W. M. C. Foulkes, J. Chem. Phys. **143**, 102807 (2015).

[18] G. Rajagopal, R. J. Needs, A. James, S. D. Kenny, and W. M. C. Foulkes, Phys. Rev. B **51**, 10591 (1995).

[19] C. Lin, F. H. Zong, and D. M. Ceperley, Phys. Rev. E **64**, 016702 (2001).

[20] H. J. Monkhorst and J. D. Pack, Phys. Rev. B **13**, 5188 (1976).

[21] M. Dagrada, S. Karakuzu, V. L. Vildosola, M. Casula, and S. Sorella, Phys. Rev. B **94**, 245108 (2016).

[22] T. N. Mihm, A. R. McIsaac, and J. J. Shepherd, J. Chem. Phys. **150**, 191101 (2019)

[23] Z. Wang, F. F. Assaad, and F. Parisen Toldin, Phys. Rev. E **96**, 042131 (2017).

[24] S. Karakuzu, K. Seki, and S. Sorella, Phys. Rev. B **98**, 075156 (2018).

[25] Y. Yang, V. Gorelov, C. Pierleoni, D. M. Ceperley, and M. Holzmann, arXiv:1910.07531.

[26] C. Gros, Phys. Rev. B **53**, 6865 (1996).

[27] G. Rajagopal, R. J. Needs, S. Kenny, W. M. C. Foulkes, and A. James, Phys. Rev. Lett. **73**, 1959 (1994).

[28] A. Baldereschi, Phys. Rev. B **7**, 5212 (1973).

[29] R. J. Needs, M. D. Towler, N. D. Drummond, and P. Lopez Rios, J. Phys.: Condens. Matter **22**, 023201 (2010).

[30] P. Giannozzi, S. Baroni, N. Bonini, M. Calandra, R. Car, C. Cavazzoni, D. Ceresoli, G. L. Chiarotti, M. Cococcioni, I. Dabo, A. Dal Corso, S. de Gironcoli, S. Fabris, G. Fratesi, R. Gebauer, U. Gerstmann, C. Gougoussis, A. Kokalj, M. Lazzeri, L. Martin-Samos, N. Marzari, F. Mauri, R. Mazzarello, S. Paolini, A. Pasquarello, L. Paulatto, C. Sbraccia, S. Scandolo, G. Sclauzero, A. P. Seitsonen, A. Smogunov, P. Umari, and

R. M. Wentzcovitch, J. Phys.: Condens. Matter **21**, 395502 (2009).

[31] J. R. Trail and R. J. Needs, J. Chem. Phys. **122**, 014112 (2005); **122**, 174109 (2005).

[32] N. D. Drummond, J. R. Trail, and R. J. Needs, Phys. Rev. B **94**, 165170 (2016).

[33] J. P. Perdew, K. Burke, and M. Ernzerhof, Phys. Rev. Lett. **77**, 3865 (1996).

[34] S. Azadi, C. Cavazzoni, and S. Sorella, Phys. Rev. B **82**, 125112 (2010).

[35] D. Alfé and M. J. Gillan, Phys. Rev. B **70**, 161101(R) (2004).

[36] C. J. Umrigar, K. G. Wilson, and J. W. Wilkins, Phys. Rev. Lett. **60**, 1719 (1988).

[37] N. D. Drummond and R. J. Needs, Phys. Rev. B **72**, 085124 (2005).

[38] J. M. McMahon and D. M. Ceperley, Phys. Rev. Lett. **106**, 165302 (2011).

[39] G. J. Ackland, M. Dunuwille, M. Martinez-Canales, I. Loa, R. Zhang, S. Sinogeikin, W. Cai, and D. Deemyad, Science **356**, 1254 (2017).

[40] E. Babaev, A. Sudbo, and N. W. Ashcroft, Nature (London) **431**, 666 (2004).

[41] J. M. McMahon, M. A. Morales, C. Pierleoni, and D. M. Ceperley, Rev. Mod. Phys. **84**, 1607 (2012).

[42] S. Azadi and W. M. C. Foulkes, Phys. Rev. B **88**, 014115 (2013).

[43] S. Azadi and T. D. Kühne, Phys. Rev. B **100**, 155103 (2019).

[44] G. Ortiz and D. M. Ceperley, Phys. Rev. Lett. **75**, 4642 (1995).